


Article

Synthesis and Structural Characterization of a Silver(I) Pyrazolato Coordination Polymer [†]

Kiyoshi Fujisawa ^{1,*} , Takuya Nemoto ¹, Yui Morishima ¹ and Daniel B. Leznoff ^{2,*}

¹ Department of Chemistry, Ibaraki University, Mito, Ibaraki 310-8512, Japan; cu_peroxo@yahoo.co.jp (T.N.); fujisawa0608@gmail.com (Y.M.)

² Department of Chemistry, Simon Fraser University, 8888 University Drive, Burnaby, BC V5A1S6, Canada

* Correspondence: kiyoshi.fujisawa.sci@vc.ibaraki.ac.jp (K.F.); dleznoff@sfu.ca (D.B.L.);

Tel.: +81-29-853-8373 (K.F.); +1-778-782-4887 (D.B.L.)

[†] Dedication: Dedicated to Professor Edward R.T. Tiekink on the occasion of his 60th birthday.

Abstract: Coinage metal(I)···metal(I) interactions are widely of interest in fields such as supramolecular assembly and unique luminescent properties, etc. Only two types of polynuclear silver(I) pyrazolato complexes have been reported, however, and no detailed spectroscopic characterizations have been reported. An unexpected synthetic method yielded a polynuclear silver(I) complex $[\text{Ag}(\mu\text{-L1Clpz})]_n$ ($\text{L1Clpz}^- = 4\text{-chloride-3,5-diisopropyl-1-pyrazolate anion}$) by the reaction of $\{[\text{Ag}(\mu\text{-L1Clpz})]_3\}_2$ with $(^n\text{Bu}_4\text{N})[\text{Ag}(\text{CN})_2]$. The obtained structure was compared with the known hexanuclear silver(I) complex $\{[\text{Ag}(\mu\text{-L1Clpz})]_3\}_2$. The Ag···Ag distances in $[\text{Ag}(\mu\text{-L1Clpz})]_n$ are slightly shorter than twice Bondi's van der Waals radius, indicating some Ag···Ag argentophilic interactions. Two Ag–N distances in $[\text{Ag}(\mu\text{-L1Clpz})]_n$ were found: 2.0760(13) and 2.0716(13) Å, and their N–Ag–N bond angles of 180.00(7)° and 179.83(5)° indicate that each silver(I) ion is coordinated by two pyrazolyl nitrogen atoms with an almost linear coordination. Every five pyrazoles point in the same direction to form a 1-D zig-zag structure. Some spectroscopic properties of $[\text{Ag}(\mu\text{-L1Clpz})]_n$ in the solid-state are different from those of $\{[\text{Ag}(\mu\text{-L1Clpz})]_3\}_2$ (especially in the absorption and emission spectra), presumably attributable to this zig-zag structure having longer but differently arranged intramolecular Ag···Ag interactions of 3.39171(17) Å. This result clearly demonstrates the different physicochemical properties in the solid-state between 1-D coordination polymer and metalacyclic trinuclear (hexanuclear) or tetranuclear silver(I) pyrazolate complexes.

Keywords: polynuclear; silver; crystal structure; pyrazolate ligand; coordination polymer



Citation: Fujisawa, K.; Nemoto, T.; Morishima, Y.; Leznoff, D.B. Synthesis and Structural Characterization of a Silver(I) Pyrazolato Coordination Polymer. *Molecules* **2021**, *26*, 1015. <https://doi.org/10.3390/molecules26041015>

Academic Editors: Vera L. M. Silva and Artur M. S. Silva

Received: 11 January 2021

Accepted: 12 February 2021

Published: 15 February 2021

Publisher's Note: MDPI stays neutral with regard to jurisdictional claims in published maps and institutional affiliations.



Copyright: © 2021 by the authors. Licensee MDPI, Basel, Switzerland. This article is an open access article distributed under the terms and conditions of the Creative Commons Attribution (CC BY) license (<https://creativecommons.org/licenses/by/4.0/>).

1. Introduction

Cyclic trinuclear complexes with monovalent coinage metal ions have been of interest to coordination chemists for three decades [1–3]. One of the ligands known to form these cyclic trinuclear complexes is pyrazolate [4–6], which is known to act as an A-frame-like bridging ligand with some metal ions, with an Npz-M-Npz linear coordination mode ($\text{pz} = \text{pyrazolate anion}, \text{C}_3\text{H}_3\text{N}_2^-$) [1–4,6–9]. Early studies in 1970 suggested that silver(I) pyrazolato complexes existed as a polymeric 1-D chain $[\text{Ag}(\text{pz})]_n$ (Figure 1, left) [10]. The structure of $[\text{Ag}(\text{pz})]_n$ was discussed in that the deprotonated pyrazolato complexes are “at least trimeric but polymeric forms cannot be excluded”, based on far-IR spectroscopy data [11]. The first structural characterization of pyrazolato complexes coordinated by coinage metal(I) ions was determined by Fackler and co-workers in 1988: their reported silver(I) pyrazolato complex had three intramolecular Ag···Ag distances of 3.306(2), 3.362(2), and 3.496(2) Å, forming a trinuclear complex $[\text{Ag}(3,5\text{-Ph}_2\text{pz})_3]$ (3,5-Ph₂pz = 3,5-diphenyl-1-pyrazolate anion) [12]. After this report, the hexanuclear complex $\{[\text{Ag}(3,5\text{-Ph}_2\text{pz})_3]\}_2$ was also reported, having one intermolecular Ag···Ag interaction of 2.9712(14) Å without any crystalline solvents [13]. This dimerization to build the hexanuclear structure can be

caused by an additional stabilization of the silver(I) ions provided by argentophilic interactions ($\text{Ag}\cdots\text{Ag}$ interactions) [14]. Subsequent ab initio powder X-ray diffraction (XRD) evidence also indicated two possibilities: silver(I) pyrazolato complexes could exist as either a coordination polymer $[\text{Ag}(\text{pz})]_n$ with an intramolecular $\text{Ag}\cdots\text{Ag}$ distance of 3.40 Å or as a dimeric trinuclear $\{[\text{Ag}(\text{pz})]_3\}_2$ structure with an intermolecular $\text{Ag}\cdots\text{Ag}$ distance of 3.431(2) Å, depending on the method of synthesis [15]. After that, the single-crystal characterization of the product made by the same synthetic method with aqueous NH_3 was reported as $[\text{Ag}(\text{pz})]_n$ with an intramolecular $\text{Ag}\cdots\text{Ag}$ (argentophilic) interaction of 3.3718(7) Å, an intermolecular $\text{Ag}\cdots\text{Ag}$ interaction of 3.2547(6) Å, and an N–Ag–N angle of 169.98° (14) (Figures S1 and S2) [16]. However, its physicochemical properties such as solid-state photoluminescence have not been reported [15,16].

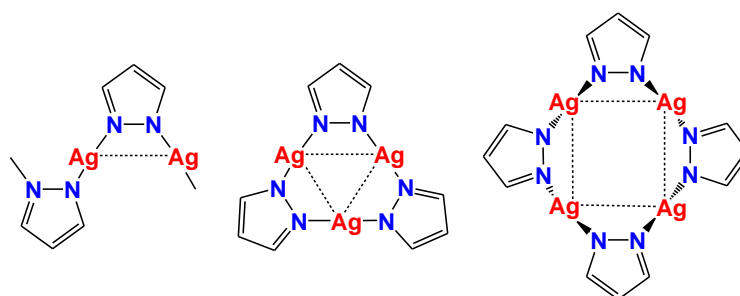


Figure 1. Schematic drawing of silver(I) pyrazolato complexes; left: polynuclear, center: trinuclear, right: tetranuclear. Dotted lines show intramolecular $\text{Ag}\cdots\text{Ag}$ interactions.

We have previously reported silver(I) pyrazolato complexes synthesized by alkyl- and aryl-substituted pyrazoles to form trinuclear and tetranuclear structures, depending on the method of synthesis and the nature of the substituents on the pyrazolate ring (Figure 1, center and right) [17–22]. Some $\text{Au}\cdots\text{Ag}$ (metallophilic) interactions in cyclic trinuclear coinage metal(I) complexes were found [1,2]. $\text{Au}\cdots\text{Im}$ complexes can be easily interacted with silver(I) ions to form $\text{Au}\cdots\text{Ag}$ interactions, since the order of π -acidity is $\text{Au} < \text{Cu} < \text{Ag}$ for a given ligand, and Im^- (imidazolate) $<$ Pyridine $<$ Cb^- (carbeniate) $<$ Pz^- for a given metal [1–3]. As an example, the mixed metal(I) complex $[(\text{Ag}\{([\text{Au}(\text{C}^2, \text{N}^3\text{-bzim})]_3)_2\})](\text{BF}_4)$ with $\text{Au}\cdots\text{Ag}$ interactions was reported ($\text{bzim}^- = 1\text{-benzylimidazole anion}$) [23].

With this electronic preference in mind, to construct $\text{Ag}\cdots\text{Ag}$ interactions by silver(I) pyrazolato complexes, it should be valuable to explore the different strategy of using electro-withdrawing substituents on the pyrazole ligand and $[\text{Ag}(\text{CN})_2]^-$ as a silver(I) ion source. The dicyanoargentate(I) anion is very useful to build coordination polymers [24–28] and performs well as a building block in general [29]. In this article, we report the detailed structure and characterizations as well as the unexpected synthetic procedure that leads to the new polynuclear silver(I) pyrazolato complex $[\text{Ag}(\mu\text{-L1Clpz})]_n$ ($\text{L1Clpz}^- = 4\text{-chloride-3,5-diisopropyl-1-pyrazolate anion}$) (Figure 2).

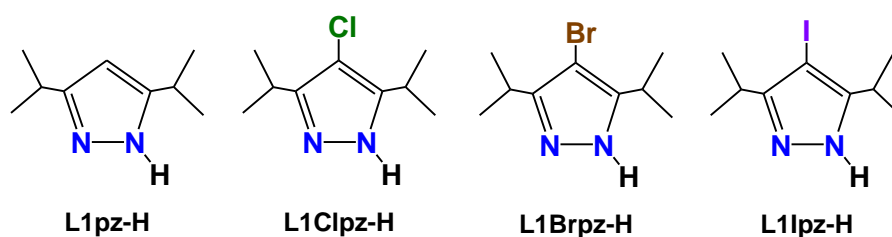


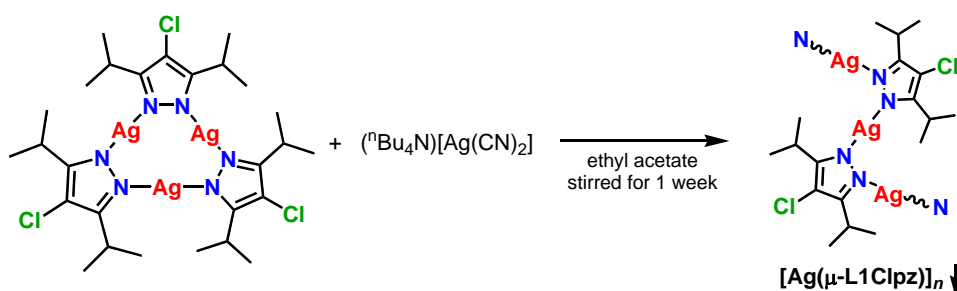
Figure 2. Pyrazoles used in this research.

2. Results and Discussion

2.1. Synthesis

The reaction of $\{[\text{Ag}(\mu\text{-L1Clpz})]_3\}_2$ with 1.5 equivalents of $(^n\text{Bu}_4\text{N})[\text{Ag}(\text{CN})_2]$ in ethyl acetate was carried out at room temperature as shown in Scheme 1. After one week of

reaction time, a white powder was gradually generated. Its IR spectroscopic measurement revealed that the $\nu(\text{C}\equiv\text{N})$ stretching peak of the starting material $(^n\text{Bu}_4\text{N})[\text{Ag}(\text{CN})_2]$ at 2141 cm^{-1} disappeared and a new complex that did not contain any cyanide was generated. From a slow liquid-liquid diffusion method, we obtained a few single-crystals to reveal the structure (see Section 2.2). The above white powders prepared in the bulk synthetic method were the same as that obtained in single-crystal form and structurally characterized (below), as confirmed by the comparison of the powder X-ray diffractogram of the powder and the powder pattern generated from the single-crystal structure, as shown in Figure S3. As mentioned in the Introduction, although a $[\text{Ag}(\mu\text{-L1Clpz})_3]/[\text{Ag}(\text{CN})_2]^-$ based polynuclear structure with intermolecular $\text{Ag}\cdots\text{Ag}$ interactions was initially targeted, only the polynuclear silver(I) complex $[\text{Ag}(\mu\text{-L1Clpz})]_n$, identified as a coordination polymer was obtained (Scheme 1); the detailed mechanism leading to this product was not explored. This coordination polymer assembly was only successfully performed by $\{[\text{Ag}(\mu\text{-L1Clpz})]_3\}_2$ but was not observed either by the non-halogenated derivative $\{[\text{Ag}(\mu\text{-L1pz})]_3\}_2$ or the other halogenated derivatives $\{[\text{Ag}(\mu\text{-L1Brpz})]_3\}_2$ and $\{[\text{Ag}(\mu\text{-L1Ipz})]_3\}_2$ (Figure 2). The reactions of these other hexanuclear complexes with $(^n\text{Bu}_4\text{N})[\text{Ag}(\text{CN})_2]$ did not produce any powder precipitate. Indeed, after all of the solvent had slowly evaporated from the reaction mixture, powder XRD measurements were carried out on the resulting residues, which indicated that no new complexes were generated: only a physical mixture of the initial starting materials, i.e., the hexanuclear complexes $\{[\text{Ag}(\text{L1Xpz})]_3\}_2$ ($\text{X} = \text{H}, \text{Br}, \text{and I}$) and $(^n\text{Bu}_4\text{N})[\text{Ag}(\text{CN})_2]$ were observed. We also tried to make polynuclear $[\text{Ag}(\mu\text{-L1Xpz})]_n$ ($\text{X} = \text{H}, \text{Cl}, \text{Br}, \text{and I}$) by the literature method by using aqueous NH_3 [15,16], but only the same hexanuclear complexes $\{[\text{Ag}(\text{L1Xpz})]_3\}_2$ ($\text{X} = \text{H}, \text{Cl}, \text{Br}, \text{and I}$) were obtained.



Scheme 1. Synthetic scheme of silver(I) coordination polymer $[\text{Ag}(\mu\text{-L1Clpz})]_n$.

2.2. Structure

Single-crystal X-ray structural analysis was performed on the polynuclear silver(I) material $[\text{Ag}(\mu\text{-L1Clpz})]_n$, the perspective drawing of which is shown in Figure 3. The relevant bond lengths (\AA) and angles ($^\circ$) are noted in the caption. The 1-D coordination polymer $[\text{Ag}(\mu\text{-L1Clpz})]_n$ and packing diagram are drawn in Figure 4 and Figure S4, respectively.

$[\text{Ag}(\mu\text{-L1Clpz})]_n$ exists as a coordination polymer with an intramolecular argentophilic distance of $\text{Ag}1\cdots\text{Ag}2$, $3.39171(17)\text{ \AA}$, which is slightly shorter than twice Bondi's van der Waals radius ($3.44\text{ \AA} = 1.72\text{ \AA} \times 2$) [30], indicating the presence of $\text{Ag}\cdots\text{Ag}$ argentophilic interactions [14]. Two $\text{Ag}\text{-N}$ distances were found: $\text{Ag}1\text{-N}1$, $2.0760(13)\text{ \AA}$ and $\text{Ag}2\text{-N}2$, $2.0716(13)\text{ \AA}$. The $\text{N}\text{-Ag}\text{-N}$ bond angles of $180.00(7)^\circ$ ($\text{N}1\text{-Ag}1\text{-N}1'$) and $179.83(5)^\circ$ ($\text{N}2'\text{-Ag}2'\text{-N}2''$) indicate that each silver(I) ion has two pyrazolyl nitrogen atoms coordinated in an almost linear fashion. Two of the pyrazolate aromatic rings are completely co-planar with a dihedral angle of 0° (between pyrazole ring 1 and 2), and another pair is twisted relative to each other, with a dihedral angle of $79.24(7)^\circ$ (between pyrazole ring 2 and 3) as shown in Figure 3. Every five pyrazole units point in the same direction, thereby forming a 1-D zig-zag structure. Each 1-D zig-zag structure is isolated and there are no significant interactions with the neighboring zig-zag chain. Within each 1-D zig-zag structure, two additional $\text{Ag}\cdots\text{Ag}$ distances are noteworthy: $\text{Ag}1\cdots\text{Ag}1\#$, $4.73335(10)\text{ \AA}$

and $\text{Ag2}\cdots\text{Ag2}'$, 6.7834(3) Å. Moreover, this zig-zag structure has two Ag-based different angles with $\text{Ag2}\cdots\text{Ag1}\cdots\text{Ag2}'$, $180.000(4)^\circ$ and $\text{Ag1}\cdots\text{Ag2}'\cdots\text{Ag1}\#$, $88.499(6)^\circ$ (Figure 3).

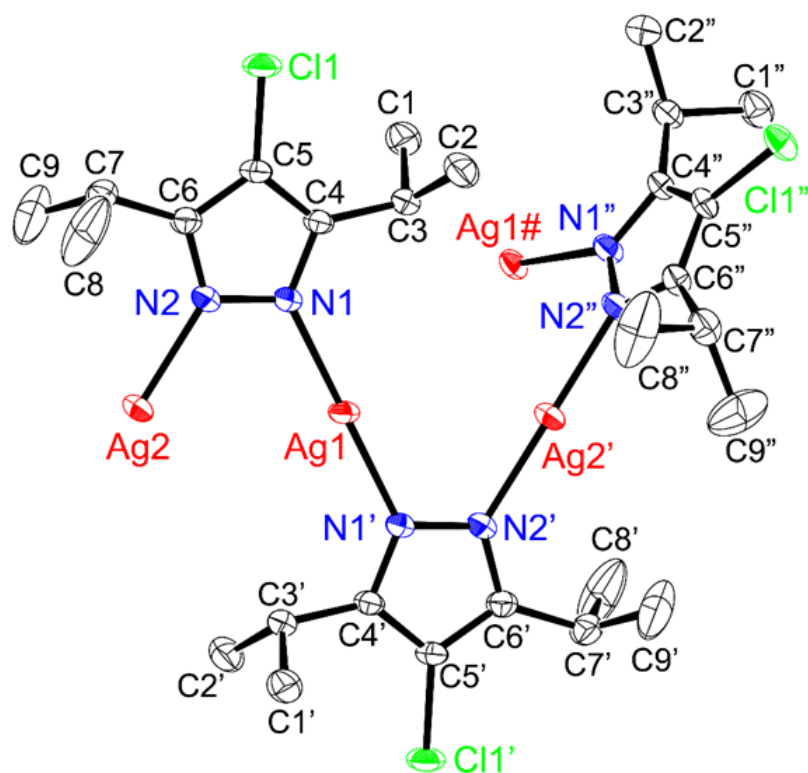


Figure 3. Crystal structure of $[\text{Ag}(\mu\text{-L1Clpz})]_n$ showing 50% displacement ellipsoids and the atom labeling scheme. Hydrogen atoms were omitted for clarity. Relevant bond lengths (Å) and angles ($^\circ$): Ag1-N1 , 2.0760(13); Ag2-N2 , 2.0716(13); $\text{Ag1-N1}'$, 2.0760(13); $\text{Ag2}'\text{-N2}'$, 2.0716(13); $\text{Ag2}'\text{-N2}''$, 2.0716(13); $\text{Ag1}\#\text{-N1}''$, 2.0760(13); N1-N2 , 1.3827(18); $\text{N1-Ag1-N1}'$, $180.00(7)$; $\text{N2-Ag2-N2}''$, $179.83(5)$; $\text{Ag1}\cdots\text{Ag2}$, 3.39171(17), $\text{Ag1}\cdots\text{Ag2}'$, 3.39171(17), $\text{Ag1}\#\cdots\text{Ag2}'$, 3.39171(17); $\text{Ag1}\cdots\text{Ag1}\#$, 4.73335(10); $\text{Ag2}\cdots\text{Ag2}'$, 6.7834(3); $\text{Ag2}\cdots\text{Ag1}\cdots\text{Ag2}'$, $180.000(4)$; $\text{Ag1}\cdots\text{Ag2}'\cdots\text{Ag1}\#$, $88.499(6)$. Symmetry codes: ', $-x+2, -y+1, -z+2$; ", $x+1, -y+1, z$; #, $-x+1/2+2, y, -z+2$.

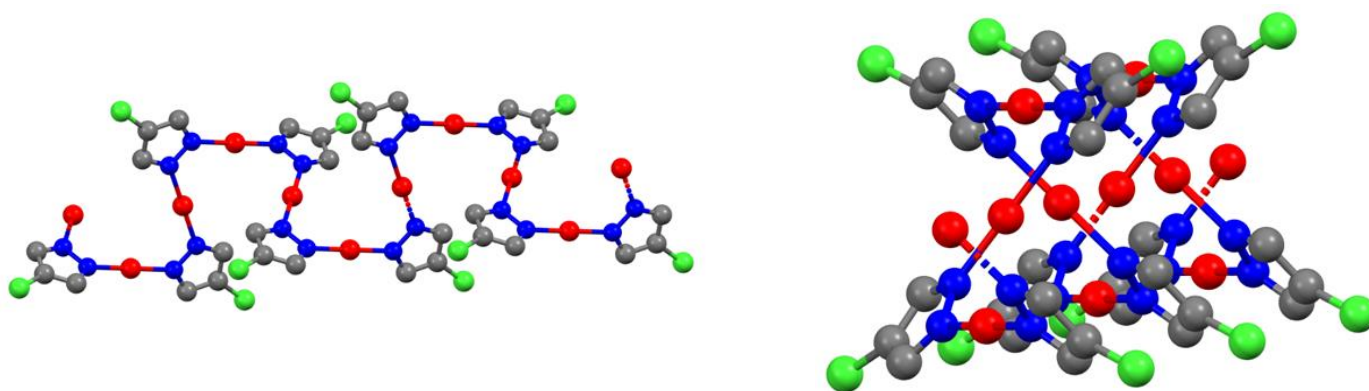


Figure 4. 1-D polynuclear structure of $[\text{Ag}(\mu\text{-L1Clpz})]_n$ (left) top view and (right) side view. Carbon atoms of isopropyl group and hydrogen atoms were omitted for clarity. Color: red, silver; blue, nitrogen; green, chlorine; grey, carbon.

This $[\text{Ag}(\mu\text{-L1Clpz})]_n$ structure is completely different from the reported one for $[\text{Ag}(\text{pz})]_n$ which exhibits an intramolecular $\text{Ag}\cdots\text{Ag}$ distance of 3.3718(7) Å. The zig-zag chain in $[\text{Ag}(\text{pz})]_n$ also interacts with neighboring zig-zag chains via inter-chain $\text{Ag}\cdots\text{Ag}$ distances of 3.2547(6) Å (Figures S1 and S2). The zig-zag structure in $[\text{Ag}(\mu\text{-L1Clpz})]_n$ is

also different from the original hexanuclear silver(I) complex $\{[\text{Ag}(\mu\text{-L1Clpz})]_3\}_2$, which features a dimeric trinuclear structure with three intermolecular argentophilic interactions of 3.1003(17), 3.1298(15), and 3.1051 Å to form an overall hexanuclear structure (Figures S5 and S6) [20]. These distances are significantly shorter than twice Bondi's van der Waals radius (3.44 Å) [30], indicating a strong $\text{Ag}\cdots\text{Ag}$ argentophilic interaction [14] (Figure S4). The layered structure of $\{[\text{Ag}(\mu\text{-L1Clpz})]_3\}_2$ did not interact with the neighboring layered one (Figure S6). The layered structure was formed with longer $\text{Ag}\cdots\text{Ag}$ distances between two $\{[\text{Ag}(\mu\text{-L1Clpz})]_3\}_2$ complexes of 7.3531(18), 7.3881(17), and 7.5258(18) Å.

2.3. Solution-State Properties

The $^1\text{H-NMR}$ spectrum of the obtained white powder $[\text{Ag}(\mu\text{-L1Clpz})]_n$ in CDCl_3 was measured (Figure S7) and the observed chemical shifts are identical to those of $\{[\text{Ag}(\mu\text{-L1Clpz})]_3\}_2$ (Table S1) [20], indicating that the supramolecular solid-state 1-D zig-zag structure of $[\text{Ag}(\mu\text{-L1Clpz})]_n$ is not stable upon dissolution, converting to form the known hexanuclear silver(I) complex $\{[\text{Ag}(\mu\text{-L1Clpz})]_3\}_2$. This observation is also supported by its solution-state UV-Vis spectrum in cyclohexane (Figure S8) and photoluminescence spectrum in cyclohexane (Figure S9). The maximum peak position in UV-Vis spectrum is 226 nm which is the same position as that of $\{[\text{Ag}(\mu\text{-L1Clpz})]_3\}_2$ (226 nm) [20]. Moreover, the emissive maximum is 307 nm (280 nm excitation), which is also the same position as that of $\{[\text{Ag}(\mu\text{-L1Clpz})]_3\}_2$. Therefore, detailed comparisons between $[\text{Ag}(\mu\text{-L1Clpz})]_n$ and $\{[\text{Ag}(\mu\text{-L1Clpz})]_3\}_2$ were carried out by solid-state spectroscopies.

2.4. Solid-State Properties

IR and Raman spectra of the $[\text{Ag}(\mu\text{-L1Clpz})]_n$ and $\{[\text{Ag}(\mu\text{-L1Clpz})]_3\}_2$ complexes are reproduced in Figures S10 and S11, respectively. The C=N stretching vibrations of 1506 cm^{-1} (IR) and of 1507 and 1495 cm^{-1} (Raman) in $[\text{Ag}(\mu\text{-L1Clpz})]_n$ are almost the same as the C=N stretching vibrations of 1505 cm^{-1} (IR) and 1495 cm^{-1} (Raman) in $\{[\text{Ag}(\mu\text{-L1Clpz})]_3\}_2$. The C-Cl stretching vibrations could be observed in the far-IR region of 587 cm^{-1} (IR) and 575 cm^{-1} (Raman) in $[\text{Ag}(\mu\text{-L1Clpz})]_n$, which are slightly shifted from 579 cm^{-1} (IR) and 573 cm^{-1} (Raman) in $\{[\text{Ag}(\mu\text{-L1Clpz})]_3\}_2$ [20], respectively. The Ag-N stretching vibration should be observed at around 510 cm^{-1} [20,21,31] and was observed at 511 cm^{-1} (Raman) in $[\text{Ag}(\mu\text{-L1Clpz})]_n$, which was the same energy at 511 cm^{-1} (Raman) in $\{[\text{Ag}(\mu\text{-L1Clpz})]_3\}_2$ [20]. These vibrational spectroscopy comparisons indicate that each stretching vibration energy is almost the same as the other, although there is a clearly measurable difference in the C-Cl stretches, consistent with the presence of intercluster $\text{Cl}\cdots\text{Cl}$ interactions in the hexanuclear system (3.852 Å) that are absent in the 1-D zig-zag chain structure.

The solid-state UV-Vis absorption spectrum of $[\text{Ag}(\mu\text{-L1Clpz})]_n$ acquired as a Nujol suspension is shown in Figure 5, along with that of $\{[\text{Ag}(\mu\text{-L1Clpz})]_3\}_2$ [20] for comparison. The characteristic absorption band at 225 nm in $\{[\text{Ag}(\mu\text{-L1Clpz})]_3\}_2$ [20] was obviously shifted to lower energy at 248 nm with a shoulder peak around 280 nm for the 1-D zig-zag structure. This is clearly different from the behavior of solution-state UV-Vis absorption spectra as shown in Figure S8. This shift in $[\text{Ag}(\mu\text{-L1Clpz})]_n$ may be caused by polynuclear formation with intramolecular argentophilic interactions of $\text{Ag}1\cdots\text{Ag}2$, 3.39171(17) Å as shown in Figure 3. For this detailed assignment, density functional theory calculations are required but are beyond the scope of this article. Nevertheless, the absorption band can be assigned to a silver(I) to pyrazolate charge transfer (MLCT) based on the other reported hexanuclear coinage metal(I) complexes [18–20,32].

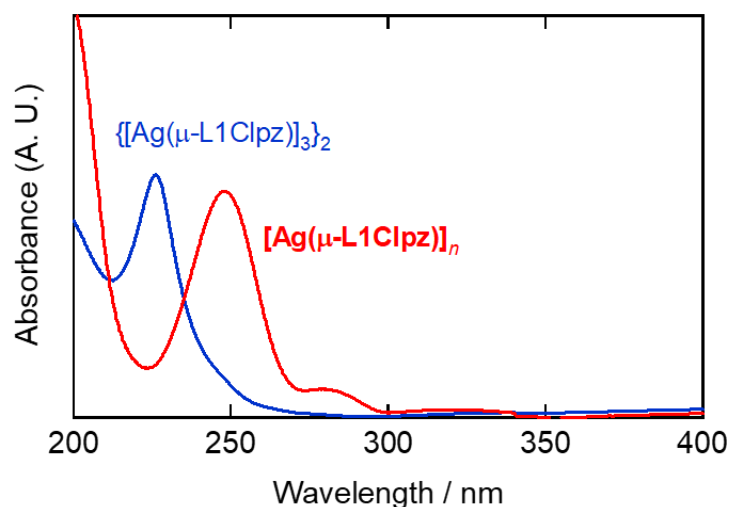


Figure 5. Solid-state UV-Vis absorption spectra of $[\text{Ag}(\mu\text{-L1Clpz})]_n$ (red line) and $\{[\text{Ag}(\mu\text{-L1Clpz})]_3\}_2$ (blue line) [20] recorded in a Nujol mull.

The emission spectrum of $[\text{Ag}(\mu\text{-L1Clpz})]_n$ in the solid-state was also somewhat different from that of the hexanuclear silver(I) analogue $\{[\text{Ag}(\mu\text{-L1Clpz})]_3\}_2$ [20] as shown in Figure 6 at room temperature, recorded using a 280 nm excitation wavelength. In $\{[\text{Ag}(\mu\text{-L1Clpz})]_3\}_2$, the main emissive band at 374 nm and an additional small one at 312 nm were observed. However, the emission of the coordination polymer $[\text{Ag}(\mu\text{-L1Clpz})]_n$ was clearly shifted to higher energy around 314 nm, and a new broad peak around 490 nm was observed.

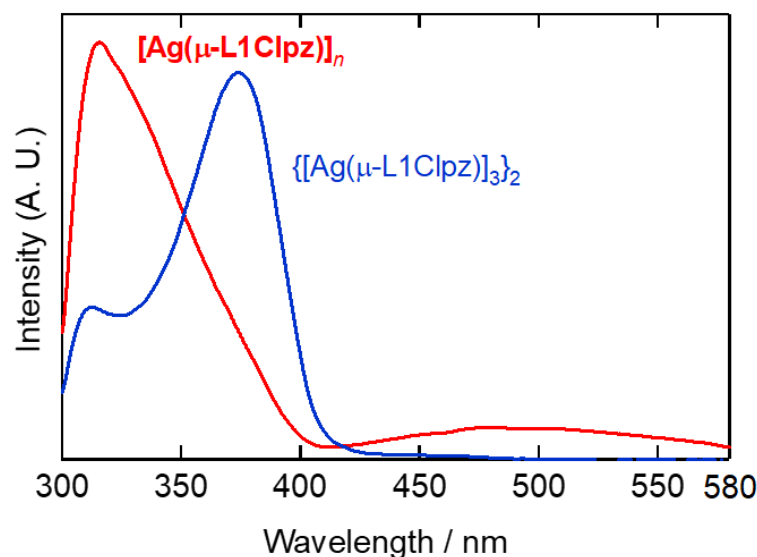


Figure 6. Solid-state photoluminescence spectra of $[\text{Ag}(\mu\text{-L1Clpz})]_n$ (red line) and $\{[\text{Ag}(\mu\text{-L1Clpz})]_3\}_2$ (blue line) [20] at room temperature recorded at 280 nm excitation wavelength.

The temperature-dependent photoluminescence spectra in $[\text{Ag}(\mu\text{-L1Clpz})]_n$ were recorded (Figure 7). The corresponding variable temperature emission spectra for $\{[\text{Ag}(\mu\text{-L1Clpz})]_3\}_2$ are also shown in Figure S12 [20]. The more intense 473 nm emission band of $[\text{Ag}(\mu\text{-L1Clpz})]_n$ at 83 K exhibited an additional vibrational fine structure around 346 nm, which was observed only at 83 K. From this vibrational behavior, this higher energy emission may be from ligand-based phosphorescence. On the other hand, the lower energy emission band was attributed to metal-based phosphorescence arising from closed shell $d^{10}\text{-}d^{10}$ intramolecular $\text{Ag}\cdots\text{Ag}$ interactions [18–21,32–34]. For the original hexanuclear complex $\{[\text{Ag}(\mu\text{-L1Clpz})]_3\}_2$, the intensity of both bands at 374 and 312 nm gradually increased as

the measurement temperature decreased. No bands around 470 nm were observed, even at low temperature. From these observations, the lower energy strong emission band at 473 nm in $[\text{Ag}(\mu\text{-L1Clpz})]_n$ is very unique due to its polynuclear supramolecular structure. We are now in the process of probing the origin of this stimulating behavior by theoretical and more detailed physicochemical researches.

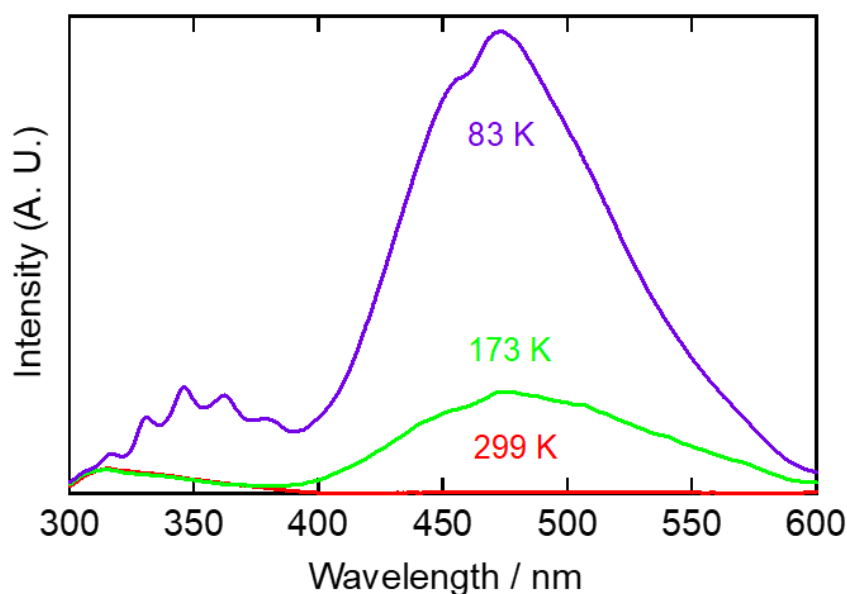


Figure 7. Solid-state temperature-dependent photoluminescence spectra at 83 K (violet line), 173 K (green line), and 299 K (red line) in $[\text{Ag}(\mu\text{-L1Clpz})]_n$ at 280 nm excitation.

3. Materials and Methods

3.1. Material and General Techniques

The preparation and handling of all complexes was performed under an argon atmosphere using standard Schlenk tube techniques. Ultra-dry ethyl acetate was purchased from Wako Pure Chemical Ind. Ltd. and deoxygenated by purging with argon gas. Deuteriochloroform was obtained from Cambridge Isotope Laboratories, Inc. Other reagents were commercially available and were used without further purification. The 3,5-diisopropyl-1-pyrazole (L1pz-H) [35] and its halogenated pyrazoles (L1Clpz-H, L1Brpz-H, and L1Ipz-H) [20] were prepared by published methods. $(^n\text{Bu}_4\text{N})[\text{Ag}(\text{CN})_2]$ was obtained by the reaction of $\text{KAg}(\text{CN})_2$ (1.016 g, 5.10 mmol) and $^n\text{Bu}_4\text{NBr}$ (1.7029 g, 5.28 mmol) in 20 mL of H_2O at room temperature for 2 hours to form a white powder of $(^n\text{Bu}_4\text{N})[\text{Ag}(\text{CN})_2]$ (1.801 g, 4.48 mmol, 88% yield). Hexanuclear silver(I) complexes ($\{[\text{Ag}(\mu\text{-L1Clpz})]_3\}_2$, $\{[\text{Ag}(\mu\text{-L1Brpz})]_3\}_2$, and $\{[\text{Ag}(\mu\text{-L1Ipz})]_3\}_2$) were obtained by the published methods [20].

3.2. Instrumentation

IR spectra ($4000\text{--}400\text{ cm}^{-1}$) and far-IR spectra ($680\text{--}150\text{ cm}^{-1}$) were recorded as KBr pellets using a JASCO FT/IR-6300 spectrophotometer and as CsI pellets using a JASCO FT/IR 6700 spectrophotometer (JASCO, Tokyo, Japan), respectively. Raman spectra ($4000\text{--}200\text{ cm}^{-1}$) were measured as powders on a JASCO RFT600 spectrophotometer with a YAG laser 600 mW (JASCO, Tokyo, Japan). Abbreviations used in the description of vibration data are as follows: s, strong; m, medium; w, weak. $^1\text{H-NMR}$ (500 MHz) spectra were obtained on a Bruker AVANCE III-500 NMR spectrometer at room temperature (298 K) in CDCl_3 (Bruker, Yokohama, Japan). ^1H chemical shifts were reported as δ values relative to residual solvent peaks. UV-Vis spectra (solution and solid, 800–200 nm) were recorded on a JASCO V-570 spectrophotometer (JASCO, Tokyo, Japan). The values of ϵ were calculated per metal(I) ion. Solid samples (mulls) for spectroscopy were prepared by finely grinding microcrystalline material into powders with a mortar and pestle and then adding mulling agents (Nujol, poly(dimethylsiloxane), viscosity 10,000 (Aldrich)) before uniformly

spreading it between quartz plates. Powder X-ray diffraction (XRD) measurements were conducted on a Rigaku SmartLab-SP/IUA X-ray diffractometer (Rigaku, Tokyo, Japan) with a Cu K α radiation ($\lambda = 1.54 \text{ \AA}$) source (40 kV, 30 mA) and a high-speed one-dimensional detector D/teX Ultra 250. The 2θ was measured in the range of $5\text{--}90^\circ$ with a scan step of 0.02° and scan speed of $10^\circ \text{ min}^{-1}$. Solid samples for XRD were prepared by finely grinding microcrystalline materials into powders with a mortar and pestle and then placing them on an aluminum dish (0.2 mm thickness). Luminescence spectra were recorded on a JASCO FP-6500 (solid, 700–300 nm) spectrofluorometer (JASCO, Tokyo, Japan). Low-temperature electronic absorption and luminescence spectra were recorded using solid samples cooled with a liquid nitrogen cryostat (CoolSpeK USP-203) from Unisoku Scientific Instruments (Osaka, Japan). The elemental analyses (C, H, and N) were performed by the Chemical Analysis Center of Ibaraki University.

3.3. Preparation of Complexes

$[\text{Ag}(\mu\text{-L1Clpz})]_n$

$\{[\text{Ag}(\mu\text{-L1Clpz})]_3\}_2$ (54.5 mg, 0.0309 mmol) and $(^n\text{Bu}_4\text{N})[\text{Ag}(\text{CN})_2]$ (19.1 mg, 0.0475 mmol) were dissolved in ethyl acetate (6 cm^3) and the solution was stirred at room temperature for one week. A white solid was precipitated during this time. After this, the white solid was filtered and washed with a small amount of ethyl acetate. The obtained white powder as $[\text{Ag}(\mu\text{-L1Clpz})]_n$ was dried by vacuum pump.

Yield: 22.7 mg, 0.077 mmol, 42%.

Calcd for $\text{C}_9\text{H}_{14}\text{AgClN}_2 \cdot 1/4(\text{H}_2\text{O})$: C, 36.27; H, 4.90; N, 9.40. Found: C, 36.21; H, 4.57; N, 9.20. IR (KBr, cm^{-1}): 2971s(C-H), 2925s(C-H), 2862s(C-H), 1506m(C \equiv N), 1461m, 1400m, 1367m, 1361m, 1283m, 1145s, 1118s, 1092s, 1051s, 1035s, 804w. Far-IR(CsI, cm^{-1}): 685w, 587m(C-Cl), 561w, 540w, 501,476w, 437w, 411w, 389w, 371w, 349w, 276w, 237br. Raman (solid, cm^{-1}): 2974s(C-H), 2913s(C-H), 2865s(C-H), 1507m(C \equiv N), 1495m(C \equiv N), 1461m, 1448m, 1430m, 1382m, 1369s, 1300m, 1283m, 1176w, 1145w, 1107m, 957w, 880m, 706w, 657m, 575m(C-Cl), 511m(Ag-N), 438w, 385w, 341w, 268m. $^1\text{H-NMR}$ (CDCl_3 , 500 MHz): δ 1.41 (d, $J = 7 \text{ Hz}$, 36H, CHMe_2), δ 3.13 (sept, $J = 7 \text{ Hz}$, 6H, CHMe_2). UV-Vis (solution, cyclohexane, $\lambda_{\text{max}}/\text{nm}(\epsilon/\text{cm}^{-1} \text{ mol}^{-1} \text{ dm}^3)$) 226 (39200). UV-Vis (solid, Nujol, nm): 248, 280 (sh). Emission at 280 nm excitation wavelength (solution, cyclohexane, $\lambda_{\text{max}}/\text{nm}$): 307. Emission at 280 nm excitation wavelength (solid, $\lambda_{\text{max}}/\text{nm}$): 299 K, 315, 490; 173 K, 314, 474, 614sh; 83 K, 317, 331, 346, 362, 379, 456sh, 473.

Liquid-liquid diffusion was applied to obtain crystals at room temperature. The $\{[\text{Ag}(\mu\text{-L1Clpz})]_3\}_2$ (0.05 mmol) in 10 mL of ethyl acetate was transferred to a 30 mL Erlenmeyer flask. On this solution, the solution containing $(^n\text{Bu}_4\text{N})[\text{Ag}(\text{CN})_2]$ (0.1 mmol) dissolved in 10 mL of ethyl acetate was carefully layered and then the top was covered by parafilm. After a few weeks, some crystals were formed, which were suitable for single-crystal X-ray analysis.

3.4. X-ray Crystal Structure Determination

Crystal data and refinement parameters for the silver(I) pyrazolato coordination polymer $[\text{Ag}(\mu\text{-L1Clpz})]_n$ are given in Table 1. All crystallographic data have been deposited at the Cambridge crystallographic data center (CCDC), 12 Union Road, Cambridge CB2 1EZ, UK and copies can be obtained on request, free of charge, by quoting the publication citation and the deposition number. CCDC number: 2053891.

The diffraction data were measured on a Rigaku/MS Mercury CCD system (Rigaku, Tokyo, Japan) with graphite monochromated Mo K α ($\lambda = 0.71070 \text{ \AA}$) radiation at -80°C . The unit cell parameters of each crystal were determined using CrystalClear [36] from 6 images. The crystal to detector distance was 44.74 mm. Data were collected using 0.5° intervals in 65° and ω to a maximum 2θ value of 55.0° . A total of 744 oscillation images were collected. The highly redundant data sets were reduced using CrysAlisPro [37]. An empirical absorption correction was applied for each complex. Structures were solved by direct methods (SIR2008) [38]. The position of the silver ions and their first coordination

sphere were located from a direct method *E*-map; other non-hydrogen atoms were found in alternating difference Fourier syntheses and least squares refinement cycles. During the final refinement cycles the temperature factors were refined anisotropically. Refinement was carried out by a full matrix least-squares method on F^2 . All calculations were performed with the CrystalStructure [39] crystallographic software package except for refinement, which was performed using SHELXL 2013 [40]. Hydrogen atoms were placed in calculated positions. Crystallographic data and structure refinement parameters including the final discrepancies (*R* and *R_w*) are listed in Table 1.

Table 1. Crystal data and structure refinement of $[\text{Ag}(\mu\text{-L1Clpz})]_n$.

Complex	$[\text{Ag}(\mu\text{-L1Clpz})]_n$
CCDC number	2053891
Empirical Formula	$\text{C}_9\text{H}_{14}\text{AgClN}_2$
Formula Weight	293.54
Crystal System	Monoclinic
Space Group	$I2/a$ (#15)
<i>a</i> /Å	9.4667(11)
<i>b</i> /Å	11.0962(3)
<i>c</i> /Å	21.5508(7)
β /°	94.859(2)
<i>V</i> /Å ³	2255.66(11)
<i>Z</i>	8
$D_{\text{calc}}/\text{g cm}^{-3}$	1.729
$\mu(\text{MoK}\alpha)/\text{cm}^{-1}$	19.771
Temperature/°C	−80
2θ range, °	6–55
Reflections collected	8801
Unique reflections	2589
R_{int}	0.0111
Number of Variables	120
Refls./Para ratio	21.57
Residuals: <i>R</i> 1 ($I > 2\sigma(I)$)	0.0155
Residuals: <i>R</i> (All reflections)	0.0167
Residuals: <i>wR</i> 2 (All reflections)	0.0406
Goodness of fit indicator	1.046
Max/min peak, /e Å ^{−3}	0.43/−0.40

$$R1 = \sum ||F_o| - |F_c|| / \sum |F_o|, wR2 = [\sum (w(F_o^2 - F_c^2)^2) / \sum w(F_o^2)^2]^{1/2}.$$

4. Conclusions

By using an unexpected synthetic method, we obtained a silver(I) pyrazolato complex $[\text{Ag}(\mu\text{-L1Clpz})]_n$ as a coordination polymer by the reaction of $\{[\text{Ag}(\mu\text{-L1Clpz})]_3\}_2$ with $(^n\text{Bu}_4\text{N})[\text{Ag}(\text{CN})_2]$. This polynuclear silver(I) structure was compared with the known hexanuclear silver(I) structure $\{[\text{Ag}(\mu\text{-L1Clpz})]_3\}_2$. Two N–Ag–N bond angles of $180.00(7)^\circ$ and $179.83(5)^\circ$ in the silver(I) coordination polymer $[\text{Ag}(\mu\text{-L1Clpz})]_n$ indicate that each silver(I) ion is coordinated by two pyrazolyl nitrogen atoms with an almost linear coordination. Every five pyrazoles point in the same direction to form a 1-D zig-zag structure. This zig-zag structure is not stable in solution, but it converts to the original hexanuclear silver(I) complex $\{[\text{Ag}(\mu\text{-L1Clpz})]_3\}_2$. In the solid-state photoluminescence spectrum, a lower energy strong emission band at 473 nm at lower temperature is very unique and attributable to the differences in polynuclear structure between the two systems. Silver(I) complexes are not generally so emissive, even at lower temperature and thus this 1-D zig-zag polynuclear structure is particularly noteworthy in coinage metal(I) pyrazolate research. This $[\text{Ag}(\mu\text{-L1Clpz})]_n$ broadens a family of silver(I) coordination polymers [24,25,41–43]. Moreover, some high antibacterial activity research using silver(I) coordination polymers are also reported [41–44]. Further efforts to probe how the structure of coinage metal(I) pyrazolates is affected by ligand and coordination environment are in progress.

Supplementary Materials: The following are available online, CIF and checkCIF report. Figure S1: 1-D polynuclear structure of $[\text{Ag}(\mu\text{-pz})]_n$, Figure S2: Packing diagram of $[\text{Ag}(\mu\text{-pz})]_n$, Figure S3: Powder X-ray diffraction spectra of $[\text{Ag}(\mu\text{-L1Clpz})]_n$ and calcd. pattern, Figure S4: Packing diagram of $[\text{Ag}(\mu\text{-L1Clpz})]_n$, Figure S5: Crystal structure of $\{[\text{Ag}(\mu\text{-L1Clpz})]_3\}_2$, Figure S6: Packing diagram of $\{[\text{Ag}(\mu\text{-L1Clpz})]_3\}_2$, Figure S7: $^1\text{H-NMR}$ spectrum of $[\text{Ag}(\mu\text{-L1Clpz})]_n$, Table S1: Comparisons of the $^1\text{H-NMR}$ chemical shifts, Figure S8: UV-Vis spectra of $[\text{Ag}(\mu\text{-L1Clpz})]_n$ and $\{[\text{Ag}(\mu\text{-L1Clpz})]_3\}_2$ in cyclohexane, Figure S9: Luminescence spectra of $[\text{Ag}(\mu\text{-L1Clpz})]_n$ and $\{[\text{Ag}(\mu\text{-L1Clpz})]_3\}_2$ in cyclohexane, Figure S10: IR spectra of $[\text{Ag}(\mu\text{-L1Clpz})]_n$ and $\{[\text{Ag}(\mu\text{-L1Clpz})]_3\}_2$, Figure S11: Raman spectra of $[\text{Ag}(\mu\text{-L1Clpz})]_n$ and $\{[\text{Ag}(\mu\text{-L1Clpz})]_3\}_2$, Figure S12: Temperature-dependent photoluminescence spectra in $\{[\text{Ag}(\mu\text{-L1Clpz})]_3\}_2$.

Author Contributions: K.F. and D.B.L. conceived and designed the project. T.N. and Y.M. performed the experiments. T.N. and K.F. analyzed the data. K.F. and D.B.L. wrote the paper. All authors have read and agreed to the published version of the manuscript.

Funding: This research received no directed/sponsored external funding.

Data Availability Statement: Data is contained within the article and supplementary material.

Acknowledgments: K.F. is grateful for the support from an Ibaraki University Priority Research Grant and the joint usage/research program "Artificial Photosynthesis" based at Osaka City University. DBL is grateful to NSERC of Canada for ongoing research support via the Discovery Grant program.

Conflicts of Interest: The authors declare no conflict of interest.

Sample Availability: Samples of the compounds $[\text{Ag}(\mu\text{-L1Clpz})]_n$ and $\{[\text{Ag}(\mu\text{-L1Clpz})]_3\}_2$ are available from the authors.

References

1. Zheng, J.; Lu, Z.; Wu, K.; Ning, G.-H.; Li, D. Coinage-metal-based cyclic trinuclear complexes with metal–metal interactions: Theories to experiments and structures to functions. *Chem. Rev.* **2020**, *120*, 9675–9742. [[CrossRef](#)] [[PubMed](#)]
2. Zheng, J.; Yang, H.; Xie, M.; Li, D. The π -acidity/basicity of cyclic trinuclear units (CTUs): From a theoretical perspective to potential applications. *Chem. Commun.* **2019**, *55*, 7134–7146. [[CrossRef](#)] [[PubMed](#)]
3. Galassi, R.; Rawashdeh-Omary, M.A.; Dias, H.V.R.; Omary, M.A. Homoleptic cyclic trinuclear d^{10} complexes: From self-association via metallophilic and excimeric bonding to the breakage thereof via oxidative addition, dative bonding, quadrupolar, and heterometal bonding interactions. *Comments Inorg. Chem.* **2019**, *39*, 287–348. [[CrossRef](#)]
4. Elguero, J.; Alkorta, I. A computational study of metallacycles formed by pyrazolate ligands and the coinage metals $M = \text{Cu(I)}$, Ag(I) and Au(I) : $(\text{pzM})_n$ for $n = 2, 3, 4, 5$ and 6 . comparison with structures reported in the Cambridge crystallographic data center (CCDC). *Molecules* **2020**, *25*, 5108. [[CrossRef](#)] [[PubMed](#)]
5. Omary, M.A.; Mohamed, A.A.; Rawashdeh-Omary, M.A.; Fackler, J.P., Jr. Photophysics of supramolecular binary stacks consisting of electron-rich trinuclear Au(I) complexes and organoelectrophiles. *Coord. Chem. Rev.* **2005**, *249*, 1372–1381. [[CrossRef](#)]
6. Zhang, J.-P.; Zhang, Y.-B.; Lin, J.-B.; Chen, X.-M. Metal azolate frameworks: From crystal engineering to functional materials. *Chem. Rev.* **2012**, *112*, 1001–1033. [[CrossRef](#)]
7. Halcrow, M.A. Pyrazoles and pyrazolides—Flexible synthons in self-assembly. *Dalton Trans.* **2009**, 2059–2073. [[CrossRef](#)]
8. Trofimenko, S. The coordination chemistry of pyrazole-derived ligands. *Chem. Rev.* **1972**, *72*, 497–509. [[CrossRef](#)]
9. Trofimenko, S. Recent advances in poly(pyrazolyl)borate (scorpionate) chemistry. *Chem. Rev.* **1993**, *93*, 943–982. [[CrossRef](#)]
10. Reimlinger, H.; Noels, A.; Jabot, J.; van Overstraeten, A. Synthesis with silver or sodium pyrazoles, I preparation of mono- and polypyrazoles. *Chem. Ber.* **1970**, *103*, 1942–1948. [[CrossRef](#)]
11. Okkersen, H.; Groeneveld, W.L.; Reedijk, J. Pyrazoles and imidazoles as ligands. Part XVIII: Neutral and anionic pyrazole coordinated to Cu(I) and Ag(I) . *Recl. Trav. Chim. Pays-Bas* **1973**, *92*, 945–953. [[CrossRef](#)]
12. Murray, H.H.; Raptis, R.G.; Fackler, J.P., Jr. Syntheses and X-ray structures of group 11 pyrazole and pyrazolate complexes. X-ray crystal structures of bis(3,5-diphenylpyrazole)copper(II) dibromide, tris(μ -3,5-diphenylpyrazolato- N,N')trisilver(I)-2-tetrahydrofuran, tris(μ -3,5-diphenylpyrazolato- N,N')trigold(I), and hexakis(μ -3,5-diphenylpyrazolato- N,N')hexagold(I). *Inorg. Chem.* **1988**, *27*, 26–33.
13. Mohamed, A.A.; Pérez, L.M.; Fackler, J.P. Jr. Unsupported intermolecular argentophilic interaction in the dimer of trinuclear silver(I) 3,5-diphenylpyrazolates. *Inorg. Chim. Acta* **2005**, *358*, 1657–1662. [[CrossRef](#)]
14. Schmidbaur, H.; Schier, A. Argentophilic interactions. *Angew. Chem. Int. Ed.* **2015**, *54*, 746–784. [[CrossRef](#)] [[PubMed](#)]
15. Masciocchi, N.; Moret, M.; Cairati, P.; Sironi, A.; Ardizzioia, G.A.; Monica, G.L. The multiphase nature of the Cu(pz) and Ag(pz) ($\text{Hpz} = \text{pyrazole}$) systems: Selective syntheses and *ab-initio* X-ray powder diffraction structural characterization of copper(I) and silver(I) pyrazolates. *J. Am. Chem. Soc.* **1994**, *116*, 7668–7676. [[CrossRef](#)]

16. Zhang, C.-Y.; Feng, J.-B.; Gao, Q.; Xie, Y.-B. *catena*-Poly[silver(I)- μ -pyrazolato- $\kappa^2N:N'$]. *Acta Cryst.* **2008**, *64*, m352. [[CrossRef](#)] [[PubMed](#)]
17. Fujisawa, K.; Okano, M.; Martín-Pastor, M.; López-Sánchez, R.; Elguero, J.; Alkorta, I. Multinuclear magnetic resonance studies of five silver(I) trinuclear pyrazolate complexes. *Struct. Chem.* **2021**, *32*, 215–224. [[CrossRef](#)]
18. Fujisawa, K.; Saotome, M.; Takeda, S.; Young, D.J. Structures and photoluminescence of coinage metal(I) phenylpyrazolato trinuclear complexes $[M(3,5-Et_2-4-Ph-pz)]_3$ and arene sandwich complexes $\{[Ag(3,5-Et_2-4-Ph-pz)]_3\}_2(Ar)$ (Ar = mesitylene and toluene). *Chem. Lett.* **2020**, *49*, 670–673. [[CrossRef](#)]
19. Saotome, M.; Shimizu, D.; Itagaki, A.; Young, D.J.; Fujisawa, K. Structures and photoluminescence of silver(I) and gold(I) cyclic trinuclear complexes with aryl substituted pyrazolates. *Chem. Lett.* **2019**, *48*, 533–536. [[CrossRef](#)]
20. Morishima, Y.; Young, D.J.; Fujisawa, K. Structure and photoluminescence of silver(I) trinuclear halopyrazolato complexes. *Dalton Trans.* **2014**, *43*, 15915–15928. [[PubMed](#)]
21. Fujisawa, K.; Ishikawa, Y.; Miyashita, Y.; Okamoto, K. Pyrazolate-bridged group 11 metal(I) complexes: Substituent effects on the supramolecular structures and physicochemical properties. *Inorg. Chim. Acta* **2010**, *363*, 2977–2989. [[CrossRef](#)]
22. Fujisawa, K.; Ishikawa, Y.; Miyashita, Y.; Okamoto, K. Crystal structure of pyrazolato-bridged copper(I) polynuclear complexes. *Chem. Lett.* **2004**, *33*, 66–67. [[CrossRef](#)]
23. Burini, A.; Bravi, R.; Fackler, J.P., Jr.; Galassi, R.; Grant, T.A.; Omary, M.A.; Pietroni, B.R.; Staples, R.J. Luminescent chains formed from neutral, triangular gold complexes sandwiching Tl^I and Ag^I . structures of $\{Ag([Au(\mu-C^2, N^3-bzim)]_3)_2\}BF_4 \cdot CH_2Cl_2$, $\{Tl([Au(\mu-C^2, N^3-bzim)]_3)_2\}PF_6 \cdot 0.5THF$ (bzim = 1-Benzylimidazolite), and $\{Tl([Au(\mu-C(OEt)=NC_6H_4CH_3)]_3)_2\}PF_6 \cdot THF$, with MAu_6 (M = Ag^+ , Tl^+) cluster cores. *Inorg. Chem.* **2000**, *39*, 3158–3165.
24. Baril-Robert, F.; Li, X.; Katz, M.J.; Geisheimer, A.R.; Leznoff, D.B.; Patterson, H. Changes in electronic properties of polymeric one-dimensional $\{[M(CN)_2]^- \}_n$ (M = Au, Ag) chains due to neighboring closed-shell Zn(II) or open-shell Cu(II) ions. *Inorg. Chem.* **2011**, *50*, 231–237. [[CrossRef](#)] [[PubMed](#)]
25. Shorrocks, C.J.; Xue, B.-Y.; Kim, P.B.; Batchelor, R.J.; Patrick, B.O.; Leznoff, D.B. Heterobimetallic coordination polymers incorporating $[M(CN)_2]^-$ (M = Cu, Ag) and $[Ag_2(CN)_3]^-$ units: Increasing structural dimensionality via M–M' and M...NC interactions. *Inorg. Chem.* **2002**, *41*, 6743–6753. [[CrossRef](#)]
26. Rawashdeh-Omary, M.A.; Omary, M.A.; Patterson, H.H.; Fackler, J.P., Jr. Excited-state interactions for $[Au(CN)_2]^-$ and $[Ag(CN)_2]^-$ oligomers in solution. Formation of luminescent gold–gold bonded excimers and exciplexes. *J. Am. Chem. Soc.* **2001**, *123*, 11237–11247. [[CrossRef](#)]
27. Omary, M.A.; Webb, T.R.; Assefa, Z.; Shankle, G.E.; Patterson, H.H. Crystal structure, electronic structure, and temperature-dependent Raman spectra of $Tl[Ag(CN)_2]$: Evidence for ligand-unsupported argentophilic interactions. *Inorg. Chem.* **1998**, *37*, 1380–1386. [[CrossRef](#)]
28. Omary, M.A.; Patterson, H.H. Temperature-dependent photoluminescence properties of $Tl[Ag(CN)_2]$: Formation of luminescent metal-metal-bonded inorganic exciplexes in the solid state. *Inorg. Chem.* **1998**, *37*, 1060–1066. [[CrossRef](#)]
29. Dragulescu-Andrasi, A.; Hietsoi, O.; Üngör, Ö.; Dunk, P.W.; Stubbs, V.; Arroyave, A.; Kovnir, K.; Shatruk, M. Dicyanometalates as building blocks for multinuclear iron(II) spin-crossover complexes. *Inorg. Chem.* **2019**, *58*, 11920–11926. [[CrossRef](#)]
30. Bondi, A. van der Waals volume and radii. *J. Phys. Chem.* **1964**, *68*, 441–451. [[CrossRef](#)]
31. Nakamoto, K. *Infrared and Raman spectra of inorganic and coordination compounds*, 6th ed.; John Wiley and Sons, Inc.: New York, NY, USA, 2009.
32. Omary, M.A.; Rawashdeh-Omary, M.A.; Gonser, M.W.A.; Elbjeirami, O.; Grimes, T.; Cundari, T.R.; Diyabalanage, H.V.K.; Gamage, C.S.P.; Dias, H.V.R. Metal Effect on the supramolecular structure, photophysics, and acid-base character of trinuclear pyrazolato coinage metal complexes. *Inorg. Chem.* **2005**, *44*, 8200–8210. [[CrossRef](#)] [[PubMed](#)]
33. Grimes, T.; Omary, M.A.; Dias, H.V.R.; Cundari, T.R. Intertrimer and intratrimer metallophilic and excimeric bonding in the ground and phosphorescent states of trinuclear coinage metal pyrazolates: A computational study. *J. Phys. Chem. A* **2006**, *110*, 5823–5830. [[CrossRef](#)] [[PubMed](#)]
34. Hettiarachchi, C.V.; Rawashdeh-Omary, M.A.; Korir, D.; Kohistani, J.; Yousufuddin, M.; Dias, H.V.R. Trinuclear copper(I) and silver(I) adducts of 4-chloro-3,5-bis(trifluoromethyl)pyrazolate and 4-bromo-3,5-bis(trifluoromethyl)pyrazolate. *Inorg. Chem.* **2013**, *52*, 13576–13583. [[CrossRef](#)]
35. Kitajima, N.; Fujisawa, K.; Fujimoto, C.; Moro-oka, Y.; Hashimoto, S.; Kitagawa, T.; Toriumi, T.; Tatsumi, K.; Nakamura, A. A new model for dioxygen binding in hemocyanin. Synthesis, characterization, and molecular structure of the μ - η^2 : η^2 peroxo dinuclear copper(II) complexes, $[Cu(HB(3,5-R_2pz)_3)]_2(O_2)$ (R = *i*-Pr and Ph). *J. Am. Chem. Soc.* **1992**, *114*, 1277–1291. [[CrossRef](#)]
36. *CrystalClear: Data Collection and Processing Software*; Rigaku Corporation: Tokyo, Akishima, Japan, 1999.
37. *CrysAlisPro: Data Collection and Processing Software*; Rigaku Corporation: Tokyo, Akishima, Japan, 2015.
38. Burla, M.C.; Caliandro, R.; Camalli, M.; Carrozzini, B.; Cascarano, G.L.; De Caro, L.; Giacovazzo, C.; Polidori, G.; Siliqi, D.; Spagna, R. *IL MILIONE*: A suite of computer programs for crystal structure solution of proteins. *J. Appl. Cryst.* **2007**, *40*, 609–613. [[CrossRef](#)]
39. *Crystal Structure 4.3: Crystal Structure Analysis Package*; Rigaku Corporation: Tokyo, Akishima, Japan, 2019.
40. Sheldrick, G.M. A short history of SHELX. *Acta Cryst.* **2008**, *A64*, 112–122. [[CrossRef](#)]
41. Jaros, S.W.; da Silva, M.F.C.G.; Florek, M.; Smoleński, P.; Pombeiro, A.J.L.; Kirillov, A.M. Silver(I) 1,3,5-triaza-7-phosphaadamantane coordination polymers driven by substituted glutarate and malonate building blocks: Self-assembly synthesis, structural features, and antimicrobial properties. *Inorg. Chem.* **2016**, *55*, 5886–5894. [[CrossRef](#)]

42. Lu, X.; Ye, J.; Zhang, D.; Xie, R.; Bogale, R.F.; Sun, Y.; Zhao, L.; Zhao, Q.; Ning, G. Silver carboxylate metal–organic frameworks with highly antibacterial activity and biocompatibility. *J. Inorg. Biochem.* **2014**, *138*, 114–121. [[CrossRef](#)] [[PubMed](#)]
43. Jaros, S.W.; Smoleński, P.; da Silva, M.F.C.G.; Florek, M.; Król, J.; Staroniewicz, Z.; Pombeiro, A.J.L.; Kirillov, A.M. New silver BioMOFs driven by 1,3,5-triaza-7-phosphaadamantane-7-sulfide (PTA=S): Synthesis, topological analysis and antimicrobial activity. *CrystEngComm* **2013**, *15*, 8060–8064. [[CrossRef](#)]
44. Domb, A.J.; Kunduru, K.R.; Farah, S. *Antimicrobial Materials for Biomedical Applications*; The Royal Society of Chemistry: Croydon, UK, 2019.